Appl. Phys. B 66, 719–725 (1998)

Applied Physics B
Lasers
and Optics

Characteristics of a cw monolithic $KTiOPO_4$ optical parametric oscillator

T. Ikegami, S. Slyusarev, T. Kurosu, Y. Fukuyama, S. Ohshima

National Research Laboratory of Metrology, 1-1-4, Umezono, Tsukuba-Shi, Ibaraki-Ken 305, Japan
(Fax: +81-298/50-1456, E-mail: ikegami@nrlm.go.jp)

Received: 27 January 1998/Revised version: 9 March 1998

Abstract. We developed a doubly resonant, cw monolithic optical parametric oscillator (OPO) characterized by a low threshold and stable long-term operation for use as a light source for optical frequency measurement. We used $KTiOPO_4$ as a nonlinear crystal and obtained a pump threshold of 7 mW and an output power of 6 mW for a pump power of 40 mW. The OPO operated in a single longitudinal mode pair of a signal and an idler, over 1 h without mode hopping in the free-running condition. The signal and the idler wavelengths were tunable by 1 nm by changing the crystal temperature by 20 °C. The continuous tuning of the beat frequency between the signal and the idler was achieved by temperature tuning (slow control, 80 MHz/K) and E-field tuning (fast control, 0.75 MHz/V). We demonstrated the feasibility of frequency control by phase locking the beat frequency. The beat frequency could be successfully phase locked to a signal generated by a synthesizer through the electrooptic effect of the crystal. The phase locking could be maintained over 1 h.

PACS: 42.65Yj; 42.62.Eh

The cw optical parametric oscillator (OPO) is a relatively old device, which was demonstrated just after the invention of lasers [1]. The cw-OPO has been considered as an ideal device that can generate radiation at any wavelength. The early experimental studies of the cw-OPO showed that it was very difficult to tune it and to achieve stable operation because a doubly resonant structure and extreme conditions are required to reduce the threshold [2]. After the development of tunable lasers such as dye lasers and diode lasers, less attention has been focused on the cw-OPO. Recent progress in solid-state pump lasers [3] and nonlinear crystals [4, 5], however, revised the consideration of the cw-OPO as a practical device. Several cw-OPOs using different nonlinear crystals and light sources have been demonstrated [6–10]. These studies were motivated by the fact that the dye laser is a huge system requiring a power-consuming Ar^+ laser, and the scope of diode lasers is limited to the wavelength region of interest from an industrial viewpoint. The development of high-power lasers enabled the operation of a singly resonant OPO (SRO) [11, 12]. Although tuning the SRO is simpler than tuning the doubly resonant OPO (DRO), the required pump power of roughly 5 W made it less attractive for practical application. Recently, by the adoption of the pump resonant configuration [13] or the intra-laser-cavity configuration [14], the pump threshold of the SRO decreased to about 200 mW, which made the SRO a more feasible and promising device.

Since the feasibility and excellent stability of the cw-OPO were recognized, the use of the cw-OPO in the frequency chain has been proposed [15] and demonstrated [6]. In addition, different types of all-solid-state frequency chains, which use only visible and near-IR light sources, were recently proposed [16, 17]. They essentially rely on the frequency interval division technique [16] and the optical frequency comb generator [18, 19], and require several light sources and nonlinear frequency conversion materials over a wide wavelength range in the visible and near-IR regions. These light sources must have moderate output power over 10 mW for the nonlinear frequency conversion, and very narrow spectral linewidth (10–100 kHz) for the electronic control of the optical frequency and phase. The OPO as a coherent light source has several advantages over other tunable light sources: (1) the intrinsic narrow spectral linewidth, which makes electronic control of the spectral linewidth easier, (2) a relatively high conversion efficiency (20%–30%), which makes the nonlinear frequency conversion easier, and (3) the capability to produce any wavelength with the same operating principle.

In order to develop a frequency chain of desired performance, the OPO needs to be operated continuously for over a day. The operation of $KTiOPO_4$ (KTP) DRO in a single longitudinal mode pair was successful even at the degenerate point by adopting type-II phase matching and a careful design of the cavity over 1 h [6]. Since both the signal and the idler must be in resonance condition, very high stability is required for the cavity. Therefore, we employed a semimonolithic cavity which had no mirror tilting mechanisms and succeeded in long-term operation without mode hopping for over 3 h [20]. The use of a semimonolithic cavity, however, results in the following problems. First, fine adjustment of the mirror is very difficult. Second, the conditions for the coatings become

severe when the operating condition is far from the degenerate point. At the non-degenerate point, triple-wavelength AR coating and triple-wavelength HR coating are required for the crystal and the mirrors, respectively. Third, as four surfaces (two mirrors and two crystal surfaces) are involved, the relatively large cavity loss results in a high threshold. To solve these problems, we decided to employ a monolithic cavity, in which two faces of the crystal are polished spherically.

The monolithic cavity is expected to provide the highest stability. On the other hand, its tunability is strongly limited if we adopt the angle tuning (critical) phase matching method. However, in the application to the frequency chain, wide tunability with a single crystal is not necessary. The possibility of OPO design at any designed wavelength is sufficient. From this point of view, we constructed a monolithic OPO using a type-II phase matching configuration, which is considered to operate stably even in the case of frequency degeneracy. We checked the tuning characteristics (discrete and continuous), the stability of the output power, and the feasibility of phase locking. The only monolithic cw-OPO ever reported uses 5% MgO:$LiNbO_3$ [8, 21] and congruent $LiNbO_3$ [22] as the nonlinear optical crystals in a type-I phase-matching configuration, and to date no experimental results have been reported for the other crystals with a type-II phase-matching configuration to the best of our knowledge. In this paper, the characteristics of a type-II monolithic cw OPO are described.

1 Experimental setup

Our monolithic OPO was fabricated from a KTP crystal (Litton Airtron, USA) with dimensions $3\,\text{mm} \times 3\,\text{mm} \times 8\,\text{mm}$. The crystal was designed to operate near the degenerate condition and was cut at the angles of $\theta = 90°$ and $\phi = 23°$, which are the same as those required to double a 1064-nm wavelength. The two surfaces were polished spherically with a radius of curvature of 10 mm. One surface (input side) had a coating with a high transmission at 532 nm ($T > 90\%$) and a high reflection at 1064 nm ($R > 99.9\%$). The other surface (output side) had a coating designed to have a high reflection at 532 nm ($R > 99\%$) and a transmission of $T = 0.3\%$ at 1064 nm. Therefore, the crystal was in the double-path configuration for the pump beam. The two z faces of the crystal were gold-coated to enable fast tuning of the cavity length via the electrooptic (EO) effect. The crystal was placed inside an aluminum holder, which was mounted on a thermoelectric (TE) cooler for temperature control. The TE cooler was mounted on a rotary stage and a tilt stage.

We studied the operating characteristics of our OPO using the setup shown in Fig. 1. As a pump source for the OPO, we used a monolithic Nd:YAG laser (NPRO, Lightwave Electronics Inc., USA), whose specified wavelength, output power, and spectral linewidth were 532 nm, 100 mW, and 10 kHz, respectively. The light beam from the NPRO passed through an optical isolator (IO-2-532HP, OFR, USA) and was mode matched to the OPO cavity by a pair of lenses. The two output beams generated by the OPO propagated in the same direction but had orthogonal polarizations due to the nature of type-II phase matching. A fraction of the pump beam passed through the crystal and was separated from the IR beams by a dichroic mirror. In this experiment, the z axis of the crystal was along the vertical direction and the pump

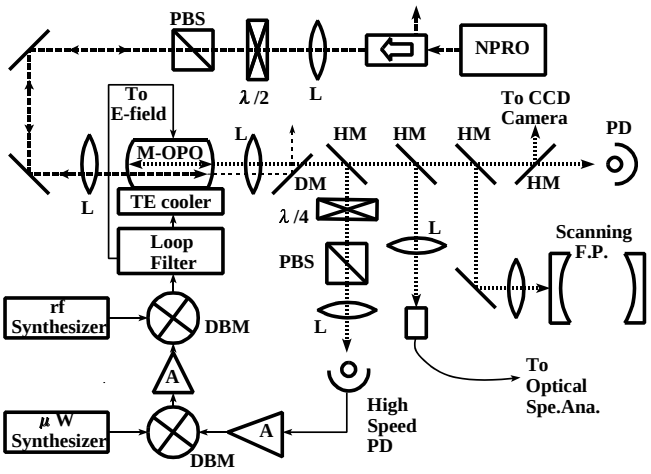

Fig. 1. Experimental setup. NPRO, monolithic Nd:YAG laser; M-OPO, monolithic OPO; L, lens; λ/2, half waveplate; PBS, polarization beam splitter; DM, dichroic mirror; HM, half mirror; PD, photodiode; DBM, double balanced mixer; A, amplifier; λ/4, quarter waveplate

wave was polarized in the horizontal plane. Here, we define the horizontally polarized wave from the OPO as a signal and the vertically polarized one as an idler. The signal and idler beams were split into five beams by four half-mirrors for diagnostics. The first beam was used to monitor the spectra at a scanning Fabry–Perot cavity with a free spectral range (FSR) of 2 GHz. The second beam was used to monitor the wavelength at an optical spectrum analyzer. The third beam was used to measure the output power at a Si PIN photodiode. The fourth beam was used to observe the transverse mode at a CCD camera. The fifth beam was detected by a high-speed photodetector with a bandwidth (BW) of 25 GHz (New Focus Inc.) to phase lock the beat frequency between the signal and the idler to a reference frequency of around 5 GHz. Since the signal and the idler beams had orthogonal polarizations, a quarter waveplate and a PBS were used to observe the beat signal.

2 Results

We obtained 7 mW of pump threshold and 6 mW of output power at a maximum pump power of 40 mW. (At the time of this experiment, the output power of the NPRO at 532 nm was 60 mW and the maximum available pump power for the OPO was 40 mW.) The output increased almost linearly from the threshold to the pump power of 40 mW. The theoretical minimum pump threshold for optimized near-field Gaussian beams for a double-path pump configuration in SI units is [23]

$$P_{\text{p,th}} = \frac{\alpha_\text{s}\alpha_\text{i} n_\text{p}^2 c\varepsilon_0 \lambda_\text{p}^3}{32\pi^2 d_\text{eff}^2 L\left(1-\delta^2\right)\overline{h}_m(B,\xi)} \quad , \tag{1}$$

where α_s, α_i are the round-trip power losses of the signal and idler fields, respectively, n_p is the refractive index of the crystal at the pump wavelength, c is the speed of light in free space, ε_0 is the electric permittivity of free space, λ_p is the pump wavelength, d_eff is the effective nonlinear coefficient,

and L is the crystal length. The degeneracy factor δ is defined as $\nu_s = \frac{1}{2}\nu_p(1+\delta)$, $\nu_i = \frac{1}{2}\nu_p(1-\delta)$, where ν_p, ν_s, ν_i are the frequencies of the pump, the signal, and the idler waves, respectively. $\overline{h}_m(B,\xi)$ is the gain reduction factor [24]. The conversion efficiency is written as [8]

$$\eta = \frac{4T}{A+T}\left(\sqrt{\frac{P_{p,th}}{P_p}} - \frac{P_{p,th}}{P_p}\right) \quad , \tag{2}$$

where P_p is the pump power. T and A are, respectively, the output mirror power transmission and internal loss (power loss fraction per round trip), assuming that they are the same for the signal and the idler field, which was approximately the case for our results as shown below. We estimated the finess for the signal and the idler field to be approximately 1300 and 1200, respectively, from the cavity resonance width using a 1064 nm Nd:YAG laser. This means that the round-trip losses including the cavity transmission are 0.48% and 0.52%, respectively. If we substitute into (1) and (2) the parameters $d_{eff} = 3.35$ (pm/V) [4], $\overline{h}_m = 0.3$, assuming $\xi = 1$, $\rho = 0.23°$ (accordingly $B = 0.57$), $A+T = 0.5\%$ and $T = 0.3\%$, we obtain a threshold of 2 mW and an efficiency of 58% at the maximum pump power. The difference between the theoretical and the experimental results might be attributed to the imperfect mode matching of the pump beam, the uncertainty in T, and the uncertainty in the double-path pump effect.

Next, we examined the tuning characteristics. Since the crystal length can be changed by the thermal expansion of the crystal, the discrete and continuous frequency tuning of the OPO can be performed by changing the temperature of the crystal. First, we start from the discrete tuning. Figure 2 shows the output power when the temperature of the crystal holder is scanned from 43 °C to 23 °C for several values of pump power. As the scanning was performed by means of natural cooling when the temperature control was switched off after the crystal holder temperature reached 43 °C, the rate of temperature change was not uniform and decreased on approaching room temperature, 23 °C. In particular, the fine structure of the resonances can be resolved at the last part of

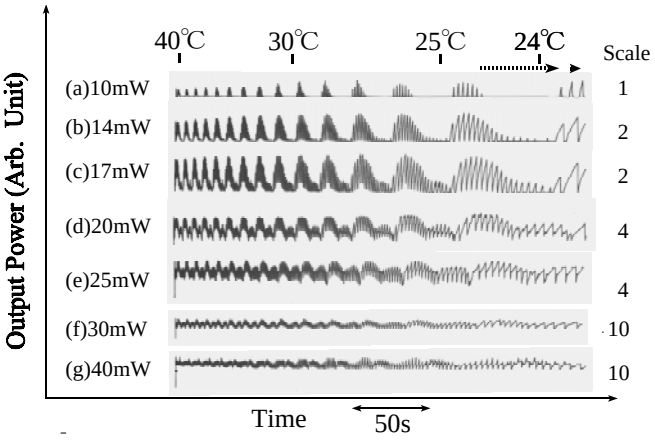

Fig. 2. The OPO output power (signal+idler) versus the crystal temperature for several pump power levels. The pump power is written at the left of each trace. 'Scale' indicates scaling of the vertical axis. The temperature was scanned from 43 °C to 23 °C with natural cooling. The temperature of the crystal holder is shown at the top of the figure

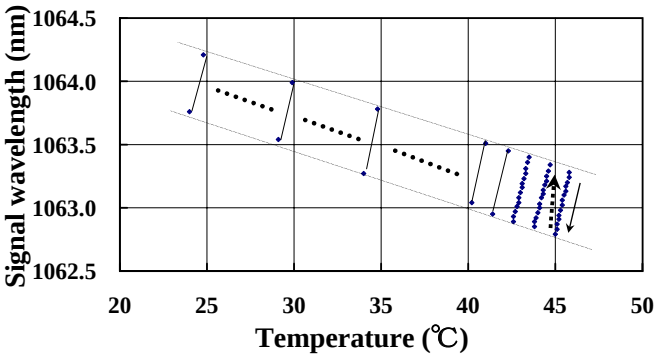

Fig. 3. Wavelength of the signal for each mode pair for the 14-mW pump. The temperature was scanned from 46 °C to 24 °C. The two *arrows* indicate the direction of the mode change. The *solid-line arrow* shows the mode hopping to the adjacent mode pair and the *dotted-line arrow* shows the cluster change

the scanning. During the temperature scan, the OPO mostly oscillated in a pair of fundamental Gaussian (TEM_{00}) modes of the signal and the idler, although oscillation in a higher-order transverse mode (TEM_{01}) was also observed a couple of times at higher pump power. Figure 3 shows the wavelength of the signal wave measured by the optical spectrum analyzer for a pump power of about 14 mW. In Fig. 3, all of the wavelengths of the oscillating signal modes are shown for only the first three groups from the high-temperature side (filled diamonds). From the fourth group, the wavelength range of the oscillating modes is connected by a thin solid line with filled diamonds at its two ends. In addition, the minimum and maximum oscillating wavelengths for each group are connected by two thin, dotted lines as a guide.

The tuning characteristics are explained as follows by assuming that the parametric gain bandwidth is smaller than the cluster spacing, which is the case for the low power pump shown in Fig. 2a,b. Since the crystal had different refractive indices for the horizontal and vertical polarizations, the simultaneous resonance for the signal and the idler modes occurs only at specific temperatures. Therefore, the temperature tuning is accompanied by mode hopping. We assume that the double-resonance condition is satisfied for a pair of signal and idler modes. If we change the temperature of the crystal, the crystal length changes as a result of thermal expansion. If the overlap in the next mode pair becomes better, the next mode pair starts to oscillate. This accompanies a frequency change of $+1\mathrm{FSR_s}$ for the signal and $-1\mathrm{FSR_i}$ for the idler. This is indicated as a thick, solid arrow in Fig. 2 and corresponds to a jump from one filled diamond to the next along the thick solid arrow in Fig. 3. When the most preferable mode pair is outside the parametric gain bandwidth, the oscillation ceases to occur, as shown in the wide gap between the groups in Fig. 2a. If we continue to scan the temperature, a wavelength jump occurs, which corresponds to a cluster spacing. This is shown by a thick dotted arrow in Figs. 2 and 3. Also, the oscillating wavelength range changes slightly because of the temperature dependence of the parametric gain bandwidth as shown by the thin dotted line in Fig. 3.

Now, we will estimate the values. From the Sellmeier equation in [4], the refractive indices for the signal and the idler wave are $n_s = 1.75$ and $n_i = 1.83$, respectively. Therefore, the FSR for the signal and the idler is $\mathrm{FSR_s} = 10.74$ GHz and $\mathrm{FSR_i} = 10.25$ GHz, respectively. When overlapping for

a mode pair is good, the next pair becomes optimum when the cavity length changes by $(\mathrm{FSR_s} - \mathrm{FSR_i})/2 = 245\,\mathrm{MHz}$. Assuming the thermal expansion coefficient α to be 1×10^{-5} /K in the crystal's xy plane [4], we find the temperature tuning coefficient of the cavity resonance frequency for the signal wave is

$$\frac{\mathrm{d}\nu_{\mathrm{s,cav}}}{\mathrm{d}T} = -\nu_{\mathrm{s,cav}}(\alpha + \frac{\mathrm{d}n_{\mathrm{s}}}{n_{\mathrm{s}}\,\mathrm{d}T}) = 4.87\,\mathrm{GHz/K} \quad ,$$

where n_{s} is the refractive index of the crystal for the signal wave (see the discussion leading to (4). Therefore, the next mode pair is more preferable when the temperature changes by $245\,\mathrm{MHz}/(4.87\,\mathrm{GHz/K}) = 50\,\mathrm{mK}$. The measured value of the temperature change between two adjacent mode pairs was 69 mK, which approximately agrees with the estimation. The cluster spacing is calculated as

$$\frac{\mathrm{FSR_s FSR_i}}{\mathrm{FSR_i} - \mathrm{FSR_s}} = 225\,\mathrm{GHz} \quad .$$

This corresponds to the $225\,\mathrm{GHz}/\mathrm{FSR_s} \simeq 21$ times mode jumps, which also agrees with the observations in Figs. 2 and 3. The wavelength for the maximum parametric gain was calculated to change by 0.05 nm/K from the same Sellmeier equation [4]. The measured slope shown by the thin, dotted line in Fig. 3 is 0.046 nm/K, which also agrees with the calculated value. By fine temperature tuning around 25 °C, we could obtain the nearly degenerate oscillation corresponding to a frequency difference between the signal and the idler of less than 1FSR . When the pump power was increased, the parametric gain bandwidth covered a couple of cluster modes and the tuning characteristics became slightly complex, as shown in Fig. 2c–g.

We observed very different behavior when the crystal was cooled and heated, especially in the case of a higher power pump. Figure 4 shows the OPO output power when the crystal temperature was scanned from 26.5 °C to 25.8 °C and in the reverse direction for (a) a 10-mW pump and (b) the maximum pump power. The direction of the scan is shown by an arrow. Before each scan, we chopped the pump beam to stop oscillation and the output power started from zero. The asymmetry of the resonance shape is clear even in the upper trace in Fig. 4a. The resonance line shape was characterized by a slow rise of the output power and a fast decrease when the crystal was cooled. When it was heated in the lower trace in Fig. 4a, the width of the resonance become much sharper. (Note the difference in the vertical scale.) The asymmetry was much more dramatic in Fig. 4b. After the scanning was stopped at 25.8 °C, the output power settled to a certain level and it exhibited stable operation for a long time. We also confirmed that the OPO oscillated stably in a single-mode pair in this state by monitoring the spectrum with the scanning FP as shown in Fig. 5. From the reverse direction scan in the lower trace in Fig. 4b, we can recognize that a couple of cluster modes are within parametric gain bandwidth.

We can qualitatively interpret this phenomenon by the thermal self-locking mechanism [25]. When we try to cool the crystal, the buildup of the OPO oscillation starts and the crystal starts to heat up because of a small amount of internal absorption. Therefore, the temperature decrease is suppressed. When the crystal is cooled further, it passes the peak resonance value and this mechanism ceases to function. On the other hand, when the crystal is heated, the heating rate is accelerated.

After the self-stabilization of the output power observed in the upper trace in Fig. 4b, stable oscillation was maintained for at least 1 h without mode hopping under the free-running condition, which is shown in Fig. 6. The phase locking mentioned in the figure is described later in this paper. We can estimate the cavity-length fluctuation (temperature fluctuation) from the observed output fluctuation. The fluctuation of the output power was estimated to be about ±3% from the upper trace in Figs. 4b and 6. The measured finess of 1300 of the OPO cavity indicates the resonance width is about 8 MHz. The fluctuation of ±3% indicates that the cavity frequency fluctuation is about $8\,\mathrm{MHz} \times 0.03 = 270\,\mathrm{kHz}$, which corresponds to the temperature fluctuation of $270\,\mathrm{kHz}/(4.87\,\mathrm{GHz/K}) = 60\,\mu\mathrm{K}$. This value corresponds to the cavity length fluctuation of 2 pm. This extremely small value appears to support the interpretation by the self-locking mechanism.

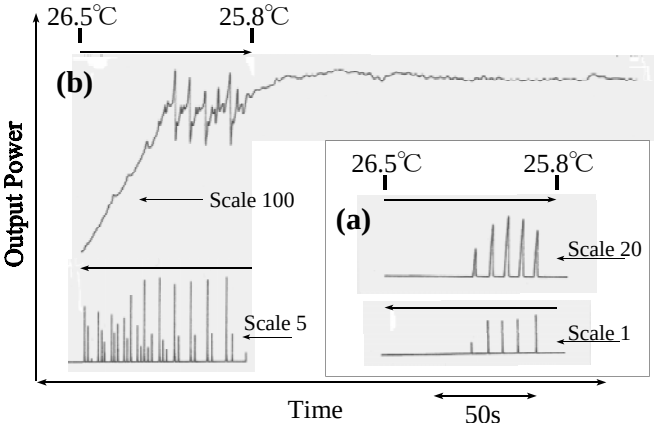

Fig. 4a,b. The detailed temperature scan for two pump power levels. **a** 10 mW pump. **b** 40 mW pump. The temperature was scanned from 26.5 °C to 25.8 °C and in the reversed direction. The direction of the scan and the start and the stop points of the scan are shown as *arrows*. 'Scale' indicates the scaling of the vertical axis

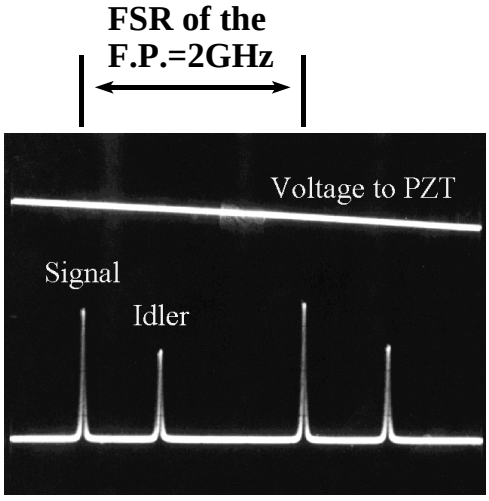

Fig. 5. The spectrum of the OPO output observed by a scanning Fabry–Perot cavity spectrum analyzer with a FSR of 2 GHz

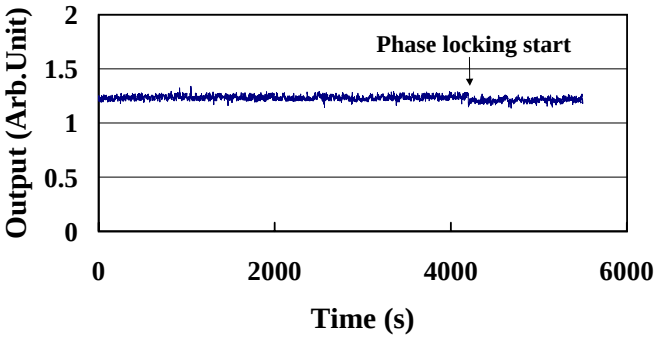

Fig. 6. The output power from the OPO under the free-running condition and the phase-locked condition. The starting point of the phase locking is shown in the figure

Next, we will focus on continuous tuning. Temperature tuning can also be used to control the frequencies of the signal and the idler continuously. However, the tuning mechanism is different from that of discrete tuning. Let us confine the discussion to one mode pair of the signal and the idler. We denote the cavity resonance frequencies for the signal and the idler waves as $\nu_{\mathrm{s,cav}}$ and $\nu_{\mathrm{i,cav}}$, respectively. When the cavity resonance frequencies change by $\Delta\nu_{\mathrm{s,cav}}$ and $\Delta\nu_{\mathrm{i,cav}}$ with a temperature variation of ΔT, the change in the oscillation frequencies of the signal ($\Delta\nu_{\mathrm{s}}$) and the idler ($\Delta\nu_{\mathrm{i}}$) are expressed as [27]

$$\Delta\nu_{\mathrm{s}} = -\Delta\nu_{\mathrm{i}} \equiv \Delta\nu = \frac{k\Delta\nu_{\mathrm{s,cav}}\mathrm{FSR_i} - \Delta\nu_{\mathrm{i,cav}}\mathrm{FSR_s}}{k\mathrm{FSR_i} + \mathrm{FSR_s}} \quad , \qquad (3)$$

where k is the ratio of the idler to signal total field loss (= the ratio of the signal to idler finess). A temperature variation changes two things: the crystal length (denoted as l_{c}) and the refractive indices. For a given crystal-length change of Δl_{c}, the effective length changes for the signal and the idler cavities are given by $n_{\mathrm{s}}\Delta l_{\mathrm{c}}$ and $n_{\mathrm{i}}\Delta l_{\mathrm{c}}$, where n_{s} and n_{i} are the refractive indices of the crystal for the signal and the idler waves, respectively. Additionally, due to the change in the refractive indices, the effective length changes are $(\Delta n_{\mathrm{s}})l_{\mathrm{c}}$ and $(\Delta n_{\mathrm{i}})l_{\mathrm{c}}$. Therefore we have, for a temperature change of ΔT,

$$\Delta\nu_{\mathrm{s,cav}} = -\nu_{\mathrm{s,cav}}\left(\alpha + \frac{\mathrm{d}n_{\mathrm{s}}}{n_{\mathrm{s}}\,\mathrm{d}T}\right) \times \Delta T \quad , \qquad (4)$$

$$\Delta\nu_{\mathrm{i,cav}} = -\nu_{\mathrm{i,cav}}\left(\alpha + \frac{\mathrm{d}n_{\mathrm{i}}}{n_{\mathrm{i}}\,\mathrm{d}T}\right) \times \Delta T \quad , \qquad (5)$$

where α is the thermal expansion coefficient, which is estimated to be 1×10^{-5} [4]. One can also estimate that $\mathrm{d}n_{\mathrm{s}}/\mathrm{d}T = 1.27\times10^{-5}$ and $\mathrm{d}n_{\mathrm{i}}/\mathrm{d}T = 1.6\times10^{-5}$ [4]. One can then obtain

$$\frac{\mathrm{d}\nu_{\mathrm{s,cav}}}{\mathrm{d}T} = -4.87\,\mathrm{GHz/K} \quad ,$$
$$\frac{\mathrm{d}\nu_{\mathrm{i,cav}}}{\mathrm{d}T} = -5.29\,\mathrm{GHz/K} \quad . \qquad (6)$$

From the measured finess for the signal and the idler, k was estimated to be $k = 1.1$. Substituting these values into (3), we then get $\mathrm{d}\nu_{\mathrm{s}}/\mathrm{d}T = 87\,\mathrm{MHz/K}$. The beat-frequency change is twice that: 174 MHz/K. We observed that the tuning coefficient was 80 MHz/K, which is considerably smaller than the calculated value. The tuning is interrupted by the mode hop to the next pair and it was approximately 80 MHz, which was the maximum continuous tuning range of the monolithic OPO.

We observed the influence of thermal self-locking during continuous tuning. When the beat frequency was changed by changing the crystal holder temperature, a strong tendency to pull it back to the original beat frequency was observed. For example, when we changed the frequency by 10 MHz, by rapidly changing the crystal holder temperature, the beat frequency settled close to the original beat frequency ($<\sim$3 MHz) in a timescale of roughly 0.1 s. The reason for the small tuning coefficient compared to the estimation might be attributed to this thermal effect.

For the application to the frequency chain, the beat frequency between the signal or the idler needs to be phase locked to a reference frequency from a synthesizer. For this purpose, the OPO must have a fast frequency control channel wider than the spectral linewidth of the free-running OPO. This is provided by the application of an E field across the crystal because the EO coefficient is different for the signal and the idler owing to the type-II phase matching even at the frequency degeneracy. The tuning coefficient of the beat frequency between the signal and the idler by E-field tuning was measured to be about 0.75 MHz/V. The tuning range limited by the applicable voltage to the crystal is considered to be around 7 MHz. Theoretically, the E-field tuning coefficients for the signal and the idler mode are calculated to be $\Delta\nu_{\mathrm{s,cav}} = -2.1\,\mathrm{MHz}\times E_z(\mathrm{V}/3\,\mathrm{mm})$ and $\Delta\nu_{\mathrm{i,cav}} = -5.7\,\mathrm{MHz}\times E_z(\mathrm{V}/3\,\mathrm{mm})$ by using the E-field-dependent refractive indices for the signal and the idler [4],

$$n_{\mathrm{s}} \simeq \left(\frac{\sin^2\phi}{n_x^2} + \frac{\cos^2\phi}{n_y^2}\right)^{-1/2} \times \left(1 - \frac{1}{2}\frac{r_{13}\sin^2\phi + r_{23}\cos^2\phi}{\frac{\sin^2\phi}{n_x^2} + \frac{\cos^2\phi}{n_y^2}}E_z\right) \quad , \qquad (7)$$

$$n_{\mathrm{i}} \simeq n_z - \frac{1}{2}n_3^3 r_{33}E_z, \qquad (8)$$

where n_x, n_y, n_z are the principal refractive indices, and r_{13}, r_{23}, r_{33} are the electrooptic constants. By inserting them into (3), the tuning coefficient for the beat frequency between the signal and the idler is calculated to be 3.41 MHz/V. The difference between the estimated and the measured values might be due to the electrical contact of the electrodes.

Finally, we actually tried to phase lock the beat frequency between the signal and the idler to a signal from a microwave synthesizer for the application of the frequency chain. As already explained, we could operate it close to the degeneracy as shown in Fig. 3 and we could observe the beat signal between the signal and the idler in the microwave frequency range (note that the FSR for our monolithic OPO is about 10 GHz). Although the walkoff angle between the signal and the idler is not zero owing to the nature of the critical-angle tuning phase matching, the separation of the signal and the idler beams at the output was not noticeable and we could easily obtain the beat signal. Even under the free-running condition, the beat frequency was very stable and its fluctuations were smaller than ±2 MHz. By detecting the beat signal with a high-speed photodetector, mixing it with a sig-

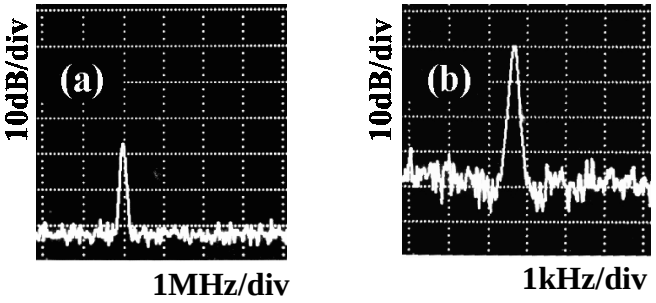

Fig. 7a,b. The beat spectrum between the signal and the idler. **a** Free running; resolution BW = 100 kHz, **b** Phase locked; resolution BW = 100 Hz

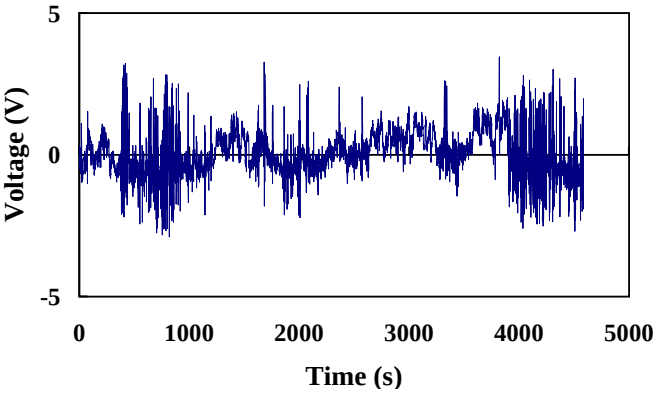

Fig. 8. The voltage applied across the crystal for phase locking

nal from microwave and rf synthesizers, and by feeding back the output from the phase detector to the E field applied to the crystal, we could obtain the phase locking of the beat signal as shown in Fig. 7. The beat frequency was about 5 GHz at this time. In Fig. 7b the phase noise level at 1–3 kHz from the carrier is approximately −35 dBc with a resolution bandwidth of 100 Hz, which yields a power spectral density of the phase noise of $\sim 2\,\mathrm{mrad}/\sqrt{\mathrm{Hz}}$ under the phase-locked condition. Figure 8 shows the control voltage applied to the crystal under the phase-locked condition and it is seen that only ±3.5 V was necessary to maintain the phase-locking condition for a long time, which is considered to be the safe voltage for the KTP crystal [26]. The control voltage of 1 V corresponded to a phase error of 0.39 rad. Because the observed maximum phase error of $3.5\,\mathrm{V} \times 0.39\,\mathrm{rad/V} = 1.37$ rad is not so small compared with $\pi/2 = 1.57$ rad, improved control might be required for longer-term operation. Since the phase error becomes zero when the lock-off of the phase locking occurs, this result is also interpreted to be the continuous monitoring of the non-existence of the mode hopping. Therefore, the minimum time of continuous operation without mode hopping in this experiment is considered to be about 1 h. In addition, phase locking did not introduce any additional fluctuations in the output power as shown in Fig. 6.

3 Conclusion

Our results are summarized as follows.

1. We fabricated a monolithic cw-OPO with a KTP crystal in a type-II, critical phase matching configuration.
2. The tuning characteristics were examined in detail. Discrete tuning by 1 nm was possible by changing the crystal temperature. Continuous tuning was also possible by applying the temperature and the E-field tuning across the crystal.
3. The monolithic cw-OPO stably oscillated in a single longitudinal mode pair for a long time even under the free-running condition owing to the thermal self-locking mechanism.
4. By using temperature tuning with a wide tunability and fast E-field tuning, we could phase lock the beat signal between the signal and the idler to a signal from a synthesizer. This did not cause lock-off during the observation time of over 1 h.

We demonstrated that the monolithic OPO can be used as a practical light source for the frequency chain. Recently, the spectral narrowing of the NPRO and the stabilization of its frequency to sub-Hz levels have been reported [28–32]. Also, the injection locking of a 10 W Nd:YAG slave laser to the NPRO was demonstrated [33]. In addition, over 1 W of cw radiation is available at 532 nm, which is produced by second-harmonic generation with a high-power Nd:YAG laser [34]. By combining these techniques, we can expect a very narrow linewidth 532-nm Nd:YAG laser as a pump source of cw-OPOs. Recently, a commercial 5-W single-frequency 532-nm source has become available (Verdi, Coherent Inc., USA). The 1-W Nd:YAG laser can pump several monolithic cw-OPOs simultaneously to produce many wavelengths with roughly 10 mW of output power. In addition, the produced signal and idler have a narrow spectral linewidth similar to the pump source. Therefore, we proposed a frequency chain which uses several cw-OPOs pumped by a single, frequency-narrowed 532-nm Nd:YAG laser [35]. Nominally, the newly proposed frequency chains require light sources in the wavelength range of over one octave [15–17]. In our case, the required range is from 800 nm to 1600 nm. Although the oscillation range of our OPO is restricted to the near-degenerate region, we can oscillate the KTP cw-OPO pumped by a 532-nm Nd:YAG laser at other wavelengths at a low threshold by cutting the KTP at an appropriate angle. If we cut the crystal in the xy plane of the crystal's refractive index ellipsoid ($\theta = 90°$), the walkoff angle is very small ($\leq 0.5°$). The phase-matching wavelength range would then be extended to 945 nm–1217 nm (a span of 272 nm) [4]. We can further extend the wavelength range to 740 nm–1893 nm (a span of 1153 nm) by using two additional KTP isomorphs, $RbTiOAsO_4$ (RTA) and $CsTiOAsO_4$ (CTA), in the xy-plane phase matching. Also, for non-degenerate operation, other crystals with type-I phase matching might be used, such as 5% MgO-doped $LiNbO_3$ [8] and periodically poled $LiNbO_4$ (PPLN) [10, 36]. As a next step, we hope to expand the wavelength span of the monolithic OPOs by using these crystals over the entire 800 nm–1600 nm range. Also, we will attempt to obtain parallel connection of several monolithic OPOs via optical-frequency comb generators [15].

Finally, the threshold for the monolithic cw-OPO is of the order of 10 mW and a laser diode can be used to pump it [37]. It can produce tunable light in the near-IR range, where at present no good light source exists.

References

1. R.G. Smith et al.: Appl. Phys. Lett. **12**, 308 (1968)
2. R.G. Smith: IEEE J. Quantum Electron. **QE-9**, 530 (1973)
3. T.J. Kane, R.L. Byer: Opt. Lett. **10**, 65 (1985)
4. J.D. Bierlein, H. Vanherzeele: J. Opt. Soc. Am. B **6**, 622 (1989); H. Vanherzeele, J.D. Bierlein: Opt. Lett. **17**, 982 (1992)
5. M.M. Fejer et al.: IEEE J. Quantum Electron. **28**, 2631 (1992)
6. D. Lee, N.C. Wong: J. Opt. Soc. Am. B **10**, 1659 (1993)
7. T.R. Stevenson et al.: Opt. Lett. **20**, 722 (1995)
8. G. Breitenbach et al.: J. Opt. Soc. Am. B **12**, 2095 (1995)
9. M. Scheidt et al.: Opt. Lett. **17**, 1287 (1997)
10. K. Schneider et al.: Opt. Lett. **22**, 1293 (1997)
11. S.T. Yang et al.: Opt. Lett. **19**, 475 (1994)
12. W.R. Bosenberg et al.: Opt. Lett. **21**, 1336 (1996)
13. K. Schneider et al.: Appl. Phys. B **65**, 775 (1997)
14. F.G. Colville et al.: Opt. Lett. **22**, 75 (1997)
15. N.C. Wong: Opt. Lett. **17**, 1156 (1992)
16. H.R. Telle et al.: Opt. Lett. **15**, 532 (1990)
17. K. Nakagawa et al.: Appl. Phys. B. **57**, 425 (1993)
18. M. Kourogi et al.: IEEE J. Quantum Electron. **29**, 2693 (1993)
19. L.R. Brothers et al.: Opt. Lett. **19**, 245 (1994)
20. T. Ikegami et al.: Jpn. J. Appl. Phys. **35**, 2690 (1996)
21. C.D. Nabors et al.: Opt. Lett. **14**, 1134 (1989)
22. D.K. Serkland et al.: Opt. Lett. **19**, 1046 (1994)
23. F.G. Corville et al.: Opt. Lett. **18**, 1065 (1993)
24. G.D. Boyd, D.A. Kleinman: J. Appl. Phys. **39**, 3597 (1968)
25. P.L. Hansen, P. Buchhave: Opt. Lett. **22**, 1074 (1997)
26. S. Slyusarev et al.: Jpn. J. Appl. Phys. **35**, 3459 (1996)
27. R.C. Eckardt et al.: J. Opt. Soc. Am. B **8**, 646 (1991)
28. T. Day et al.: IEEE J. Quantum Electron. **28**, 1106 (1992)
29. N. Uehara, K. Ueda: Opt. Lett. **18**, 505 (1993)
30. N.M. Sampas et al.: Opt. Lett. **18**, 947 (1993)
31. K. Nakagawa et al.: Appl. Phys. B **60**, 489 (1995)
32. G. Ruoso et al.: Opt. Commun. **133**, 259 (1997)
33. S.T. Yang et al.: Opt. Lett. **21**, 1676 (1996)
34. K. Schneider et al.: Opt. Lett. **21**, 1999 (1996)
35. T. Ikegami, S. Slyusarev: Proc. 11th European Frequency and Time Forum (1997) p. 104
36. L.E. Meyers, W.R. Bosenberg: IEEE J. Quantum Electron. **33**, 1663 (1997)
37. K.-J. Boller et al.: Quantum Semiclass. Opt. **9**(173), 1355 (1997)